Supporting Information

A luminescent antibacterial compound targeting Gram-negative bacterial membrane

Shuyu Yang[a]‡, Yifan Wu[ab]‡, Shang Chen[ac], Meirong Song[a], Ying Li[d]* and Kui Zhu[a]**

Supplementary Table 1 Antibacterial activities of TTCVP.

Strain (genotype)	Dark		Light	
	MIC (μg/mL)	MBC (μg/mL)	MIC (μg/mL)	MBC (μg/mL)
Gram-positive bacteria				
Staphylococcus aureus ATCC 29213	4	4	4	4
S. epidermidis 1	4	4	4	4
S. equorum 2	2	4	2	2
S. simulans 4	1	2	1	1
S. cephalus 215 (LZD^r +*cfr*)	2	4	1	2
MRSA T144	4	4	4	4
MRSA 1518 (*cfr*)	4	4	4	4
MRSA 1530 (*cfr*)	4	4	4	4
Enterococcus faecalis ATCC 29212	4	4	0.5	1
E. casseliflavus 4w-9 (*optrA*+*cfr*+*vanC*)	4	4	2	2
Bacillus subtilis ATCC 6051	1	1	0.5	0.5
Gram-negative bacteria				
Escherichia coli ATCC 25922	> 64	> 64	> 64	> 64
E. coli B2	> 64	> 64	> 64	> 64
Pseudomonas aeruginosa PAO1	> 64	> 64	> 64	> 64
Klebsiella pneumoniae HVKP4	> 64	> 64	> 64	> 64
Acinetobacter baumannii ATCC 17978	> 64	> 64	> 64	> 64

MRSA, methicillin-resistant *S. aureus*; *E. coli* B2 [62], MDR clinical isolate

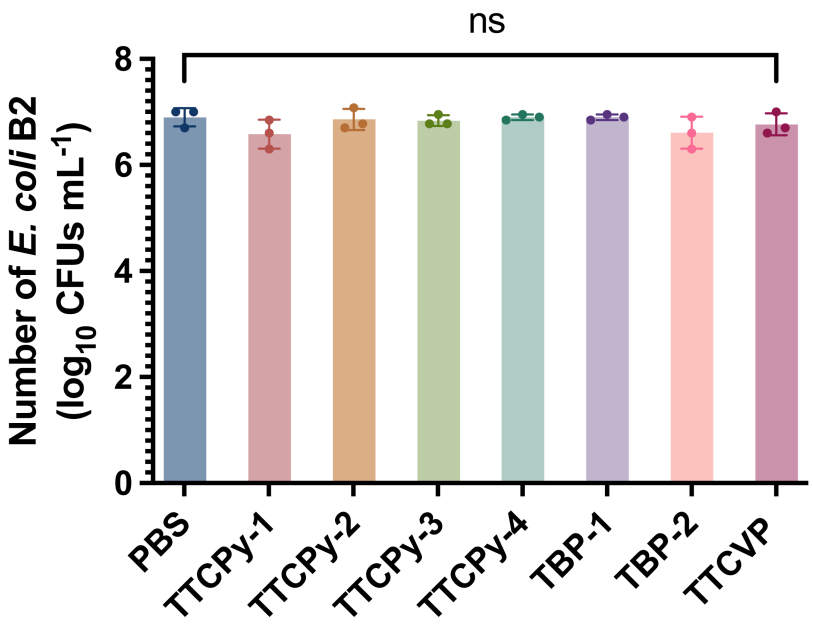

Figure S1. AIEgens exhibited no bactericidal activity against *E. coli* B2 under dark condition. The mean of three biological replicates was shown and error bars represent the s.d. P-values were determined by one-way ANOVA.

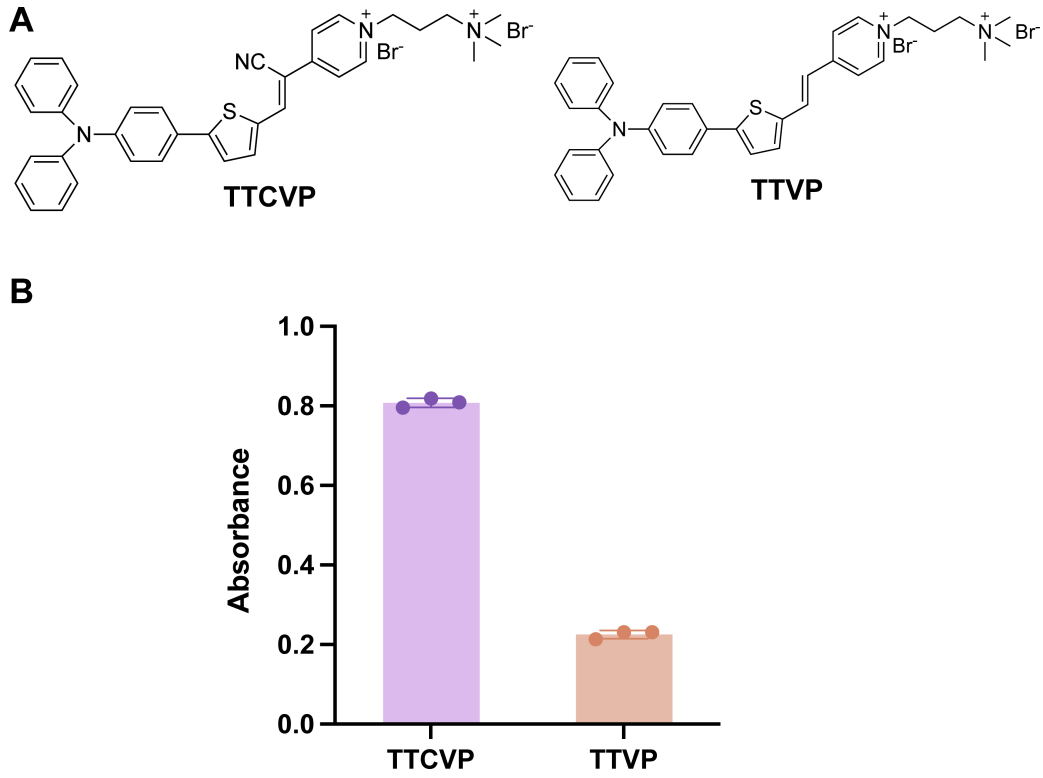

Figure S2. Aqueous solubility comparison between TTVP and TTCVP. (A) Chemical structures of TTCVP and its cyano-free analogue TTVP. (B) The aqueous solubility was evaluated by measuring the OD value at the maximum absorption peak (480 nm for TTVP and 544 nm for TTCVP) using 100-fold diluted saturated aqueous solutions. The mean of three biological replicates is shown and error bars represent the s.d.

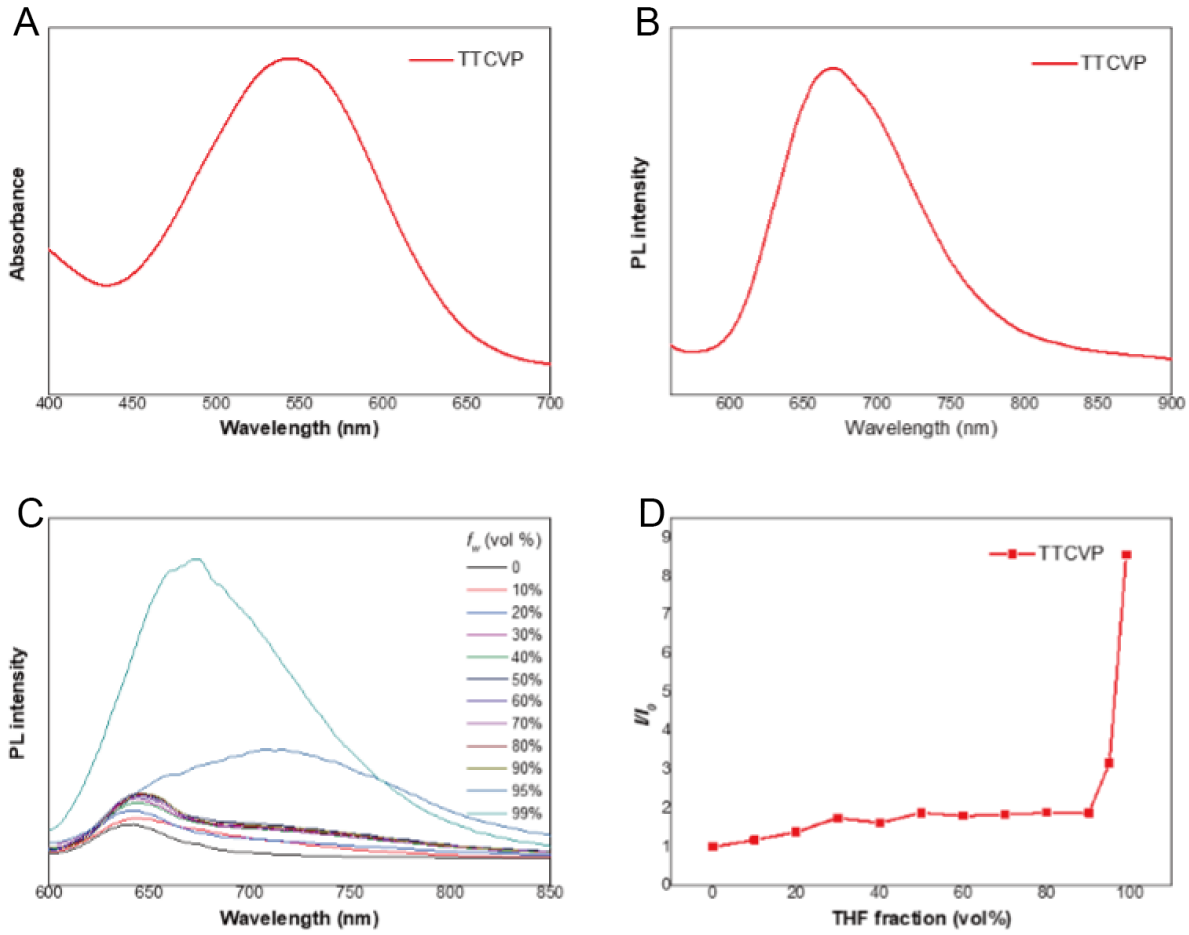

Figure S3. Photophysical Properties of TTCVP. (A) Absorption spectra of TTCVP in the DMSO solution. (B) PL spectra of TTCVP in the solid state. (C) PL spectra of TTCVP (10×10^{-6} m) in H_2O/THF mixtures with different THF fractions (f_w). (D) The plot of the relative emission intensity (I/I_0) versus the composition of the solvent mixture.

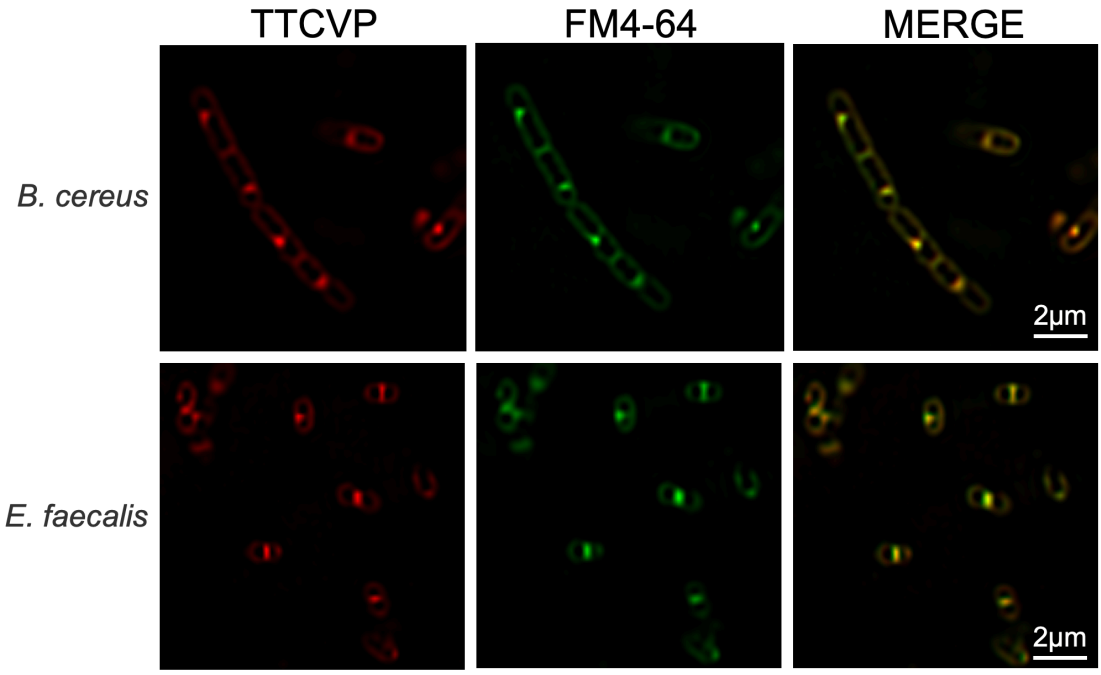

Figure S4. Ultrahigh-resolution images of *B. cereus* and *E. faecalis* incubated with TTCVP (5 μg/mL, red) and FM 4–64 (5 μg/mL, green) for 5 min. TTCVP and membrane dye FM 4–64 exhibited co-localization on bacterial membranes.

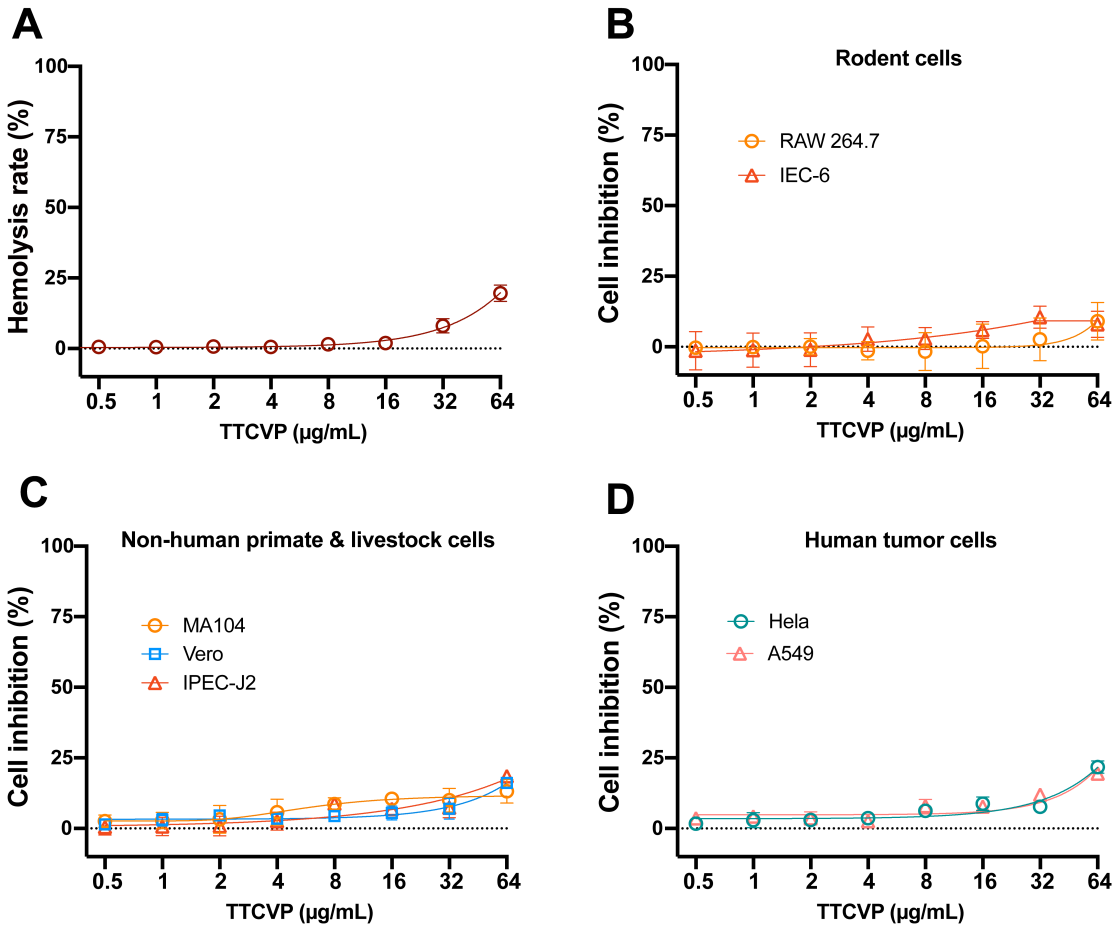

Figure S5. Safety evaluation of TTCVP. (A) Hemolysis of TTCVP. TTCVP induces hemolysis with IC_{50} of 126.8 μg/mL . (B) Cytotoxicities of TTCVP to rodent cells (RAW 264.7, IEC-6). The IC_{50} is 90.4 μg/mL for RAW 264.7 cells and 231.0 μg/mL for IEC-6 cells. (C) Cytotoxicities of TTCVP to non-human primate and livestock cells (MA104, Vero, IPEC-J2). The IC_{50} is 169.0 μg/mL for MA104 cells, 176.6 μg/mL for Vero cells and 151.8 for IPEC-J2 cells. (D) Cytotoxicities of TTCVP to human tumor cells (HeLa, A549). The IC_{50} is 100.4 μg/mL for Hela cells and 99.56 μg/mL for A549 cells. The mean of three biological replicates is shown and error bars represent the s.d.

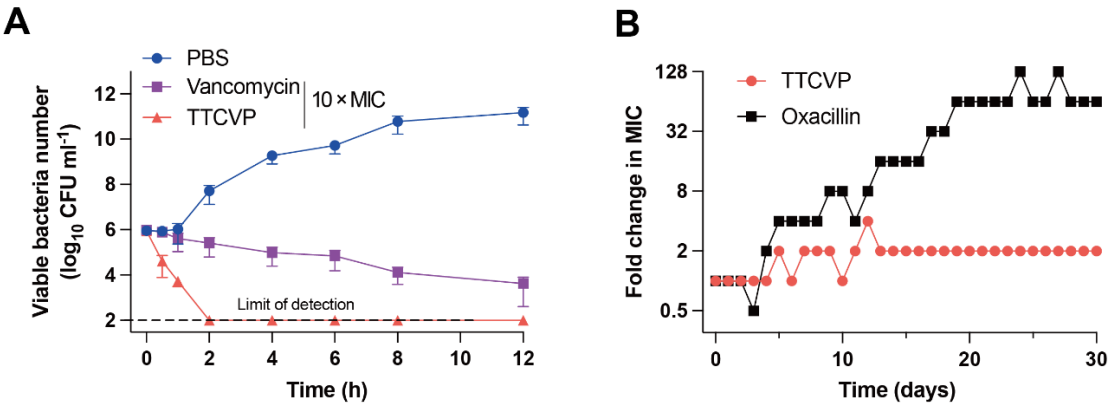

Figure S6. Antibacterial phenotype of TTCVP. (A) The time-killing curve of TTCVP against *S. aureus* ATCC 29213 in dark condition. The mean of three biological replicates is shown and error bars represent the s.d. (B) Resistance acquired during serial passage in the presence of sub-MIC levels of TTCVP and antibiotics against *S. aureus* ATCC 29213 in dark condition.

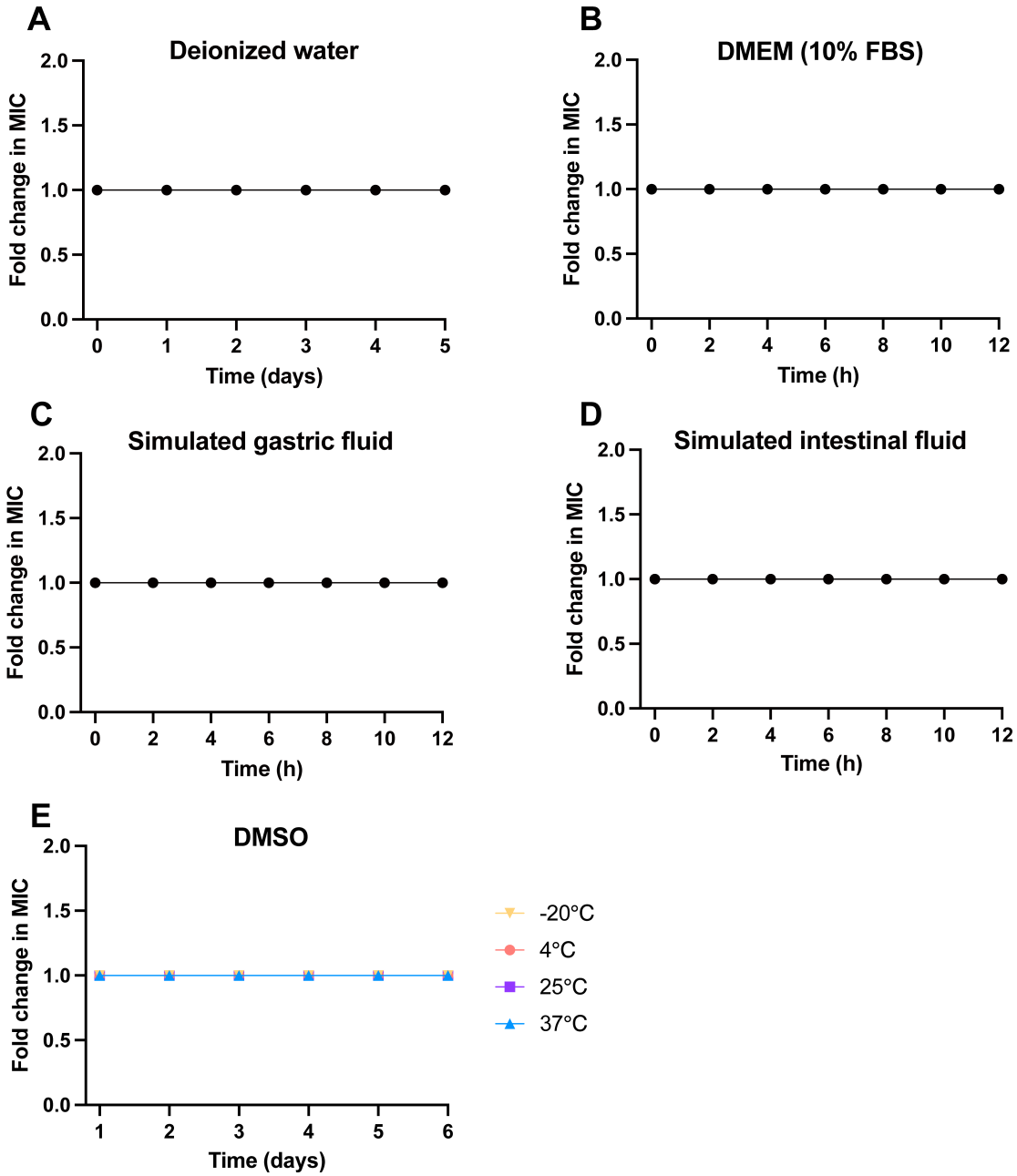

Figure S7. TTCVP exhibits excellent stability under various conditions. Fold change in MIC of TTCVP against *S. aureus* ATCC 29213 in dark condition after incubation under different conditions: (A) Deionized water for up to 5 days; (B) DMEM medium containing 10% fetal bovine serum (FBS) for up to 12 h; (C) simulated gastric fluid for up to 12 h; (D) simulated intestinal fluid for up to 12 h; and (E) DMSO at −20 °C, 4 °C, 25 °C, and 37 °C for up to 6 days. The fold change in MIC was calculated as the ratio of MIC after incubation to the initial MIC in dark condition. The mean of three biological replicates is shown and error bars represent the s.d.

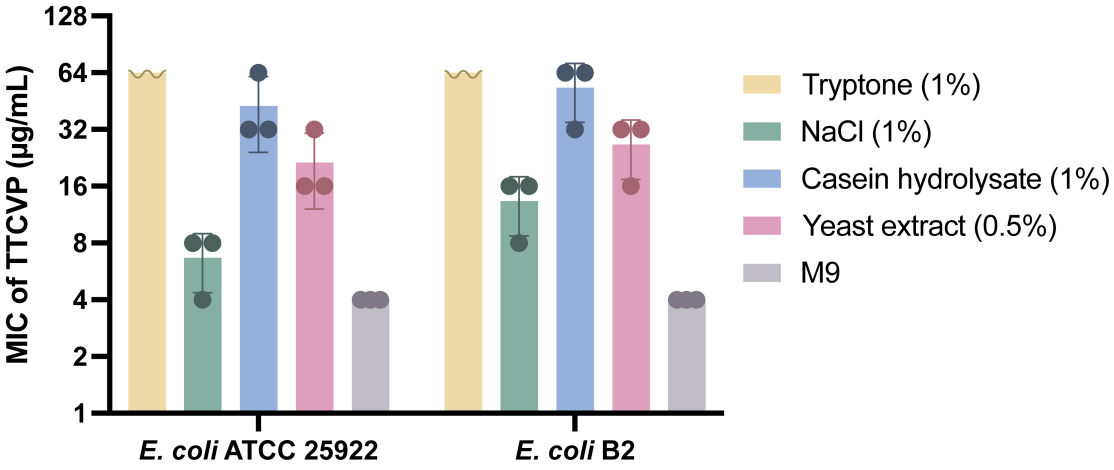

Figure S8. Medium component interference on TTCVP antibacterial activity. The MIC of TTCVP was determined in M9 minimal medium supplemented with key components from rich media (1% tryptone, 1% NaCl, 1% casein hydrolysate, 0.5% yeast extract) and compared to its activity in unmodified M9 medium in dark condition. Two *E. coli* strains, ATCC 25922 and B2, were tested. The mean of three biological replicates is shown and error bars represent the s.d.

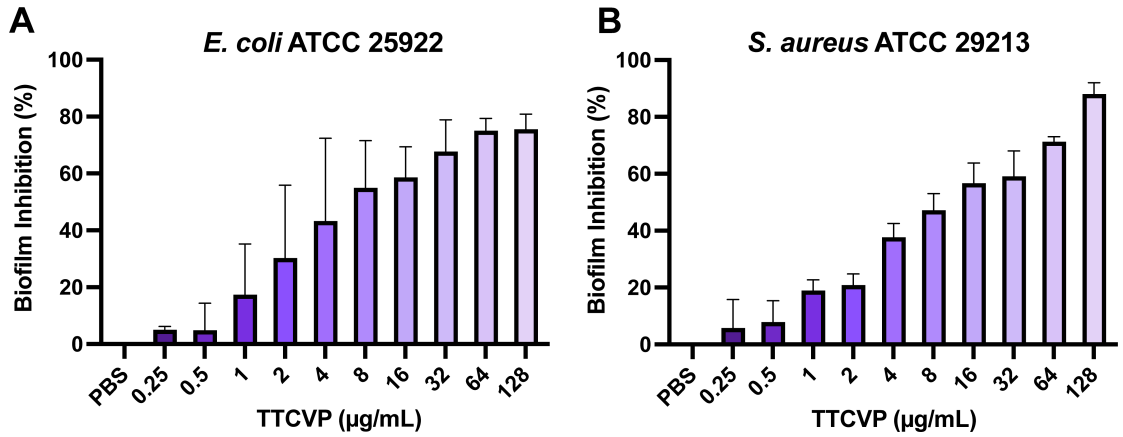

Figure S9. TTCVP inhibits bacterial biofilm formation. Biofilm inhibition rates of TTCVP against *E. coli* ATCC 25922 (A) and *S. aureus* ATCC 29213 (B) and were determined by crystal violet staining. The mean of three biological replicates is shown and error bars represent the s.d.

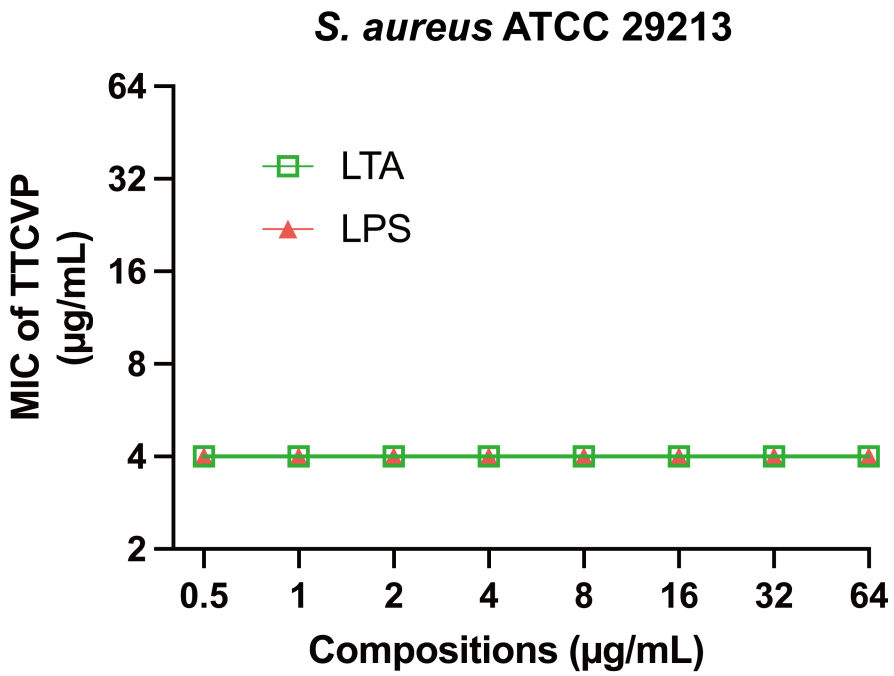

Figure S10. MIC of TTCVP with exogenous lipoteichoic acid (LTA) and LPS against *S. aureus* ATCC 29213.

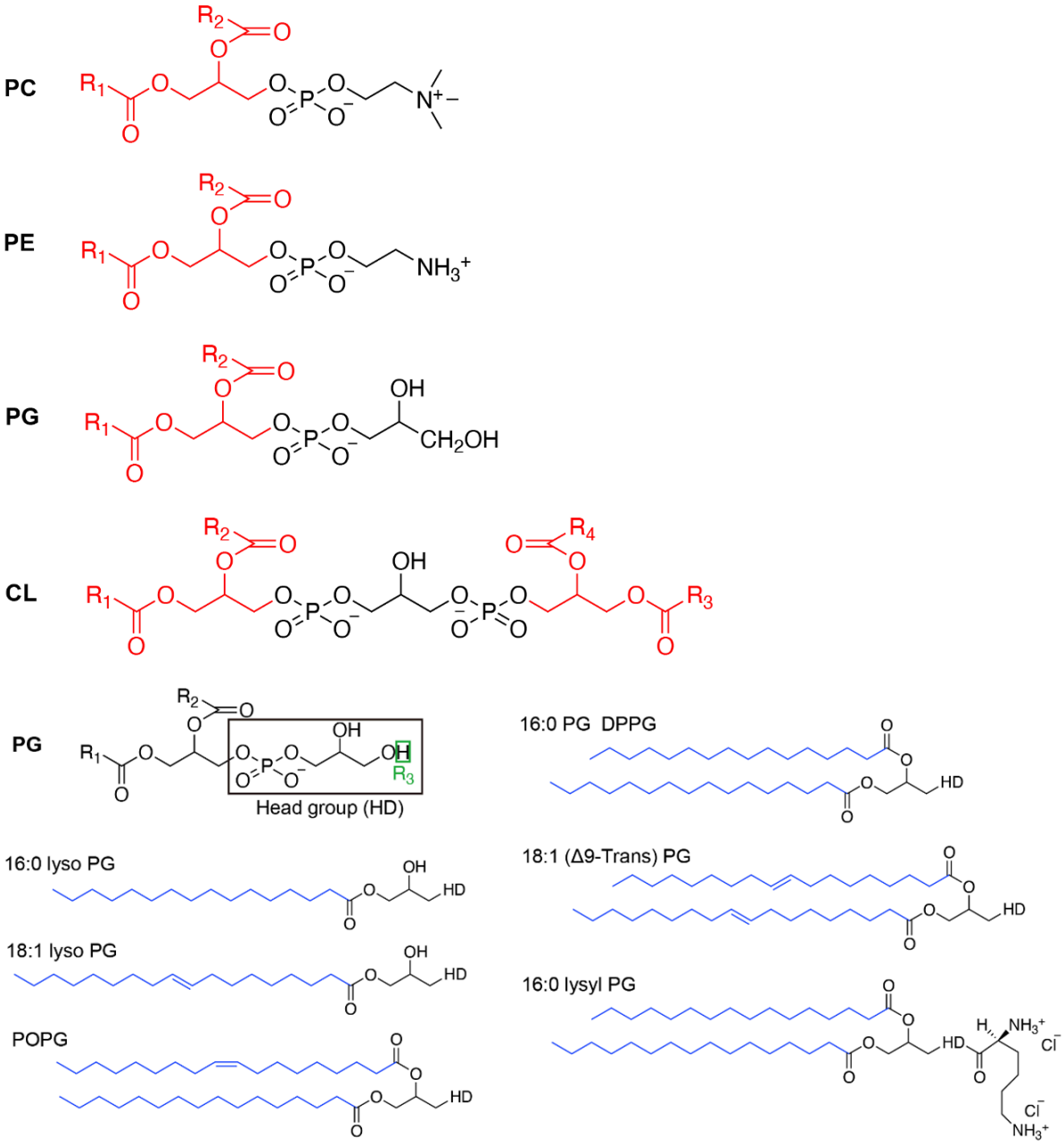

Figure S11. Structure of different bacterial membrane phospholipids. A Phospholipid. B PG.

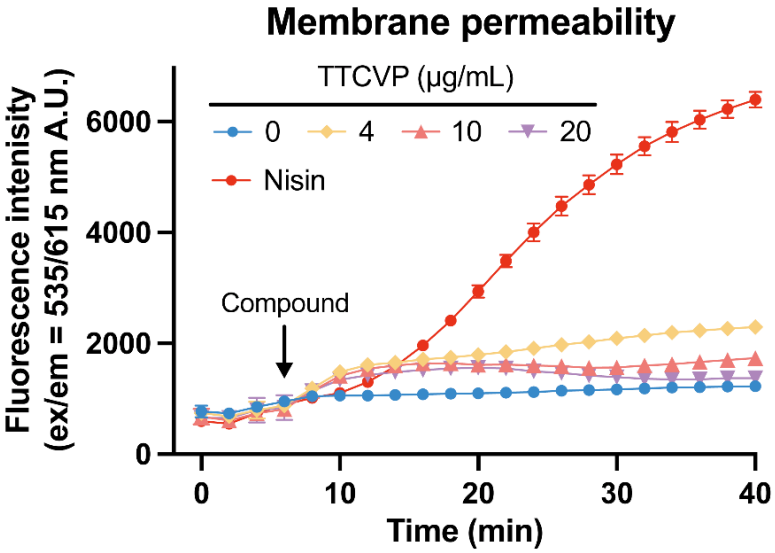

Figure S12. The membrane permeability in *S. aureus* ATCC 29213 after treated with TTCVP. The membrane permeability was probed by 10 μM PI. The arrow means the compounds were added. Nisin (100 μg/mL) was used as the positive control. The mean of three biological replicates is shown and error bars represent the s.d.

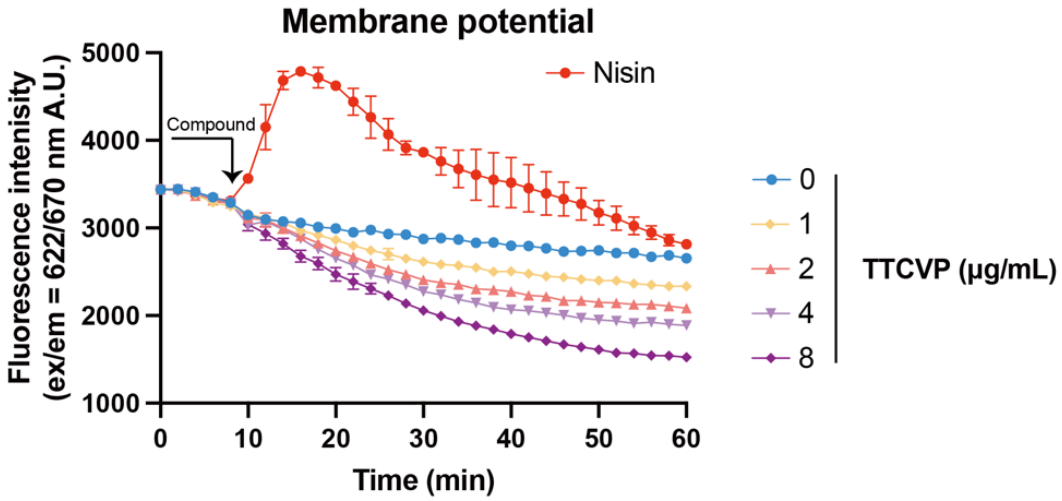

Figure S13. The membrane potential of *S. aureus* ATCC 29213 treated with TTCVP. $DiSC_3(5)$ (1 μM) was used as a fluorescence probe. Nisin (100 μg/mL) was used as the positive control. The arrow means the compounds were added at this time. The mean of three biological replicates is shown and error bars represent the s.d.

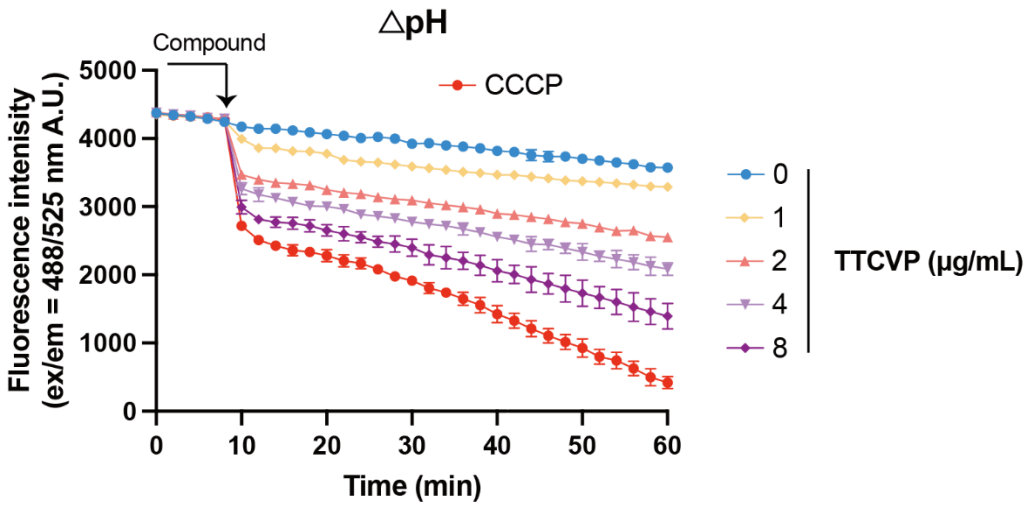

Figure S14. The ΔpH in *S. aureus* ATCC 29213 under the treatment of TTCVP probed by 10 μM BCECF-AM. CCCP (50 μM) was used as the positive control. The arrow means the compounds were added. The mean of three biological replicates is shown and error bars represent the s.d.

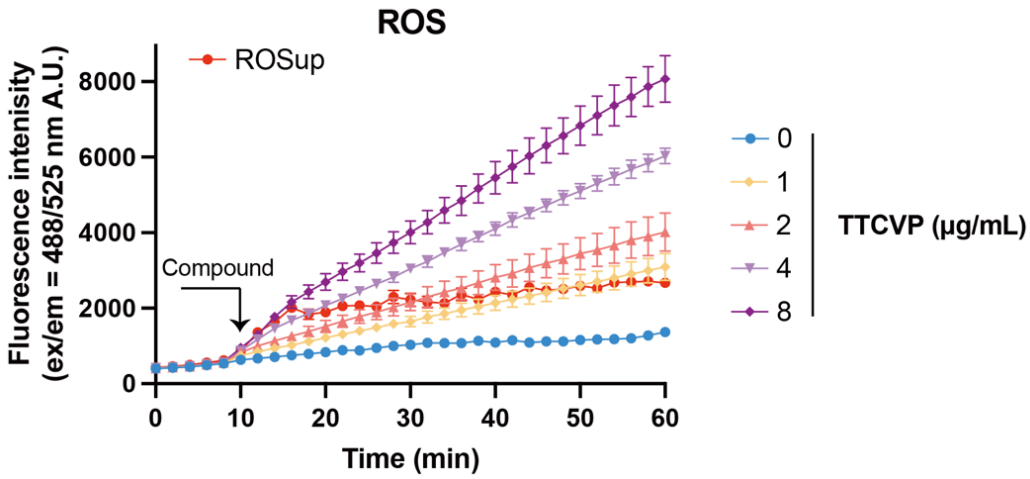

Figure S15. Total ROS accumulation in *S. aureus* ATCC 29213 after treatment with TTCVP. The arrow means the compounds were added at this time. The mean of three biological replicates is shown and error bars represent the s.d.

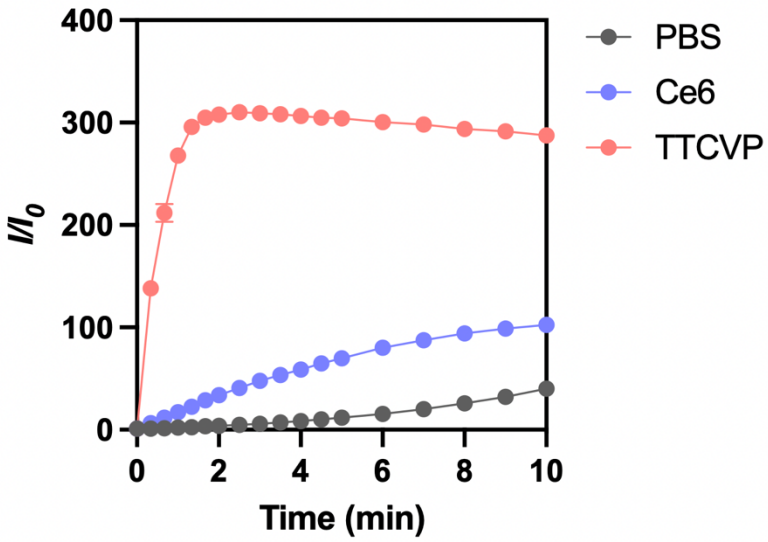

Figure S16. ROS detection in the presence of TTCVP upon white light irradiation. The plot of relative photoluminescence intensity (I/I_0) represented the ratio of the fluorescence value of the probe DCFH at a given time to the start time.

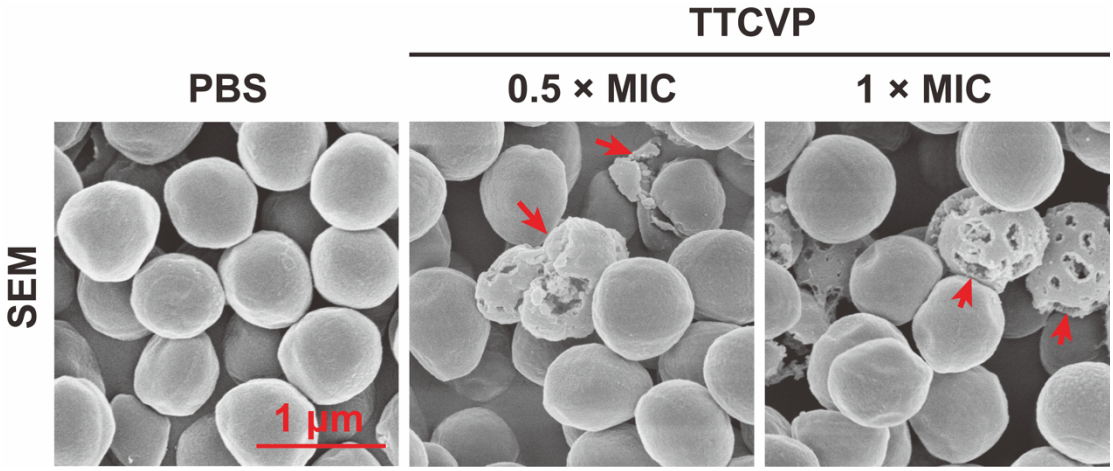

Figure S17. TTCVP induces bacterial membrane rupture and pore formation. Representative SEM images of *S. aureus* ATCC 29213 treated with PBS (control, left), 0.5× MIC of TTCVP (middle), and 1× MIC of TTCVP (right). Red arrows highlight membrane rupture and pore formation on bacterial surfaces, indicative of severe membrane damage. Scale bar: 1 μm.

A

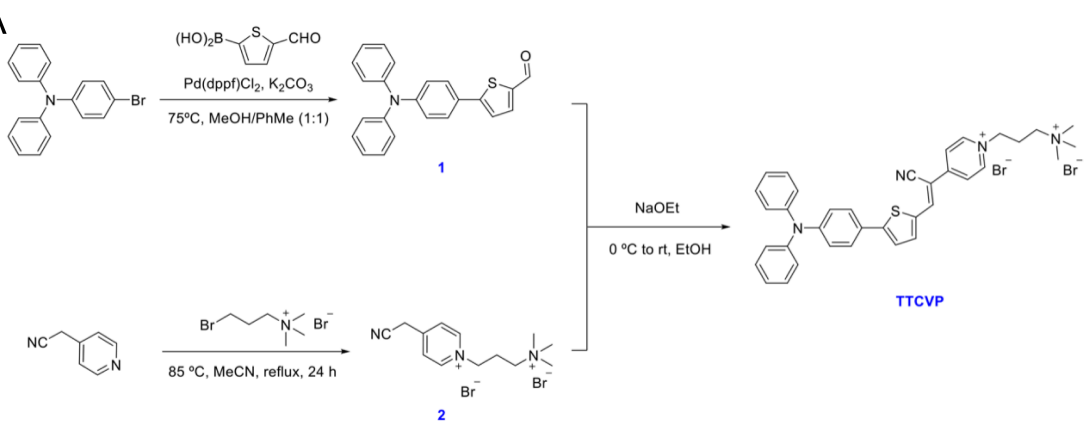

B

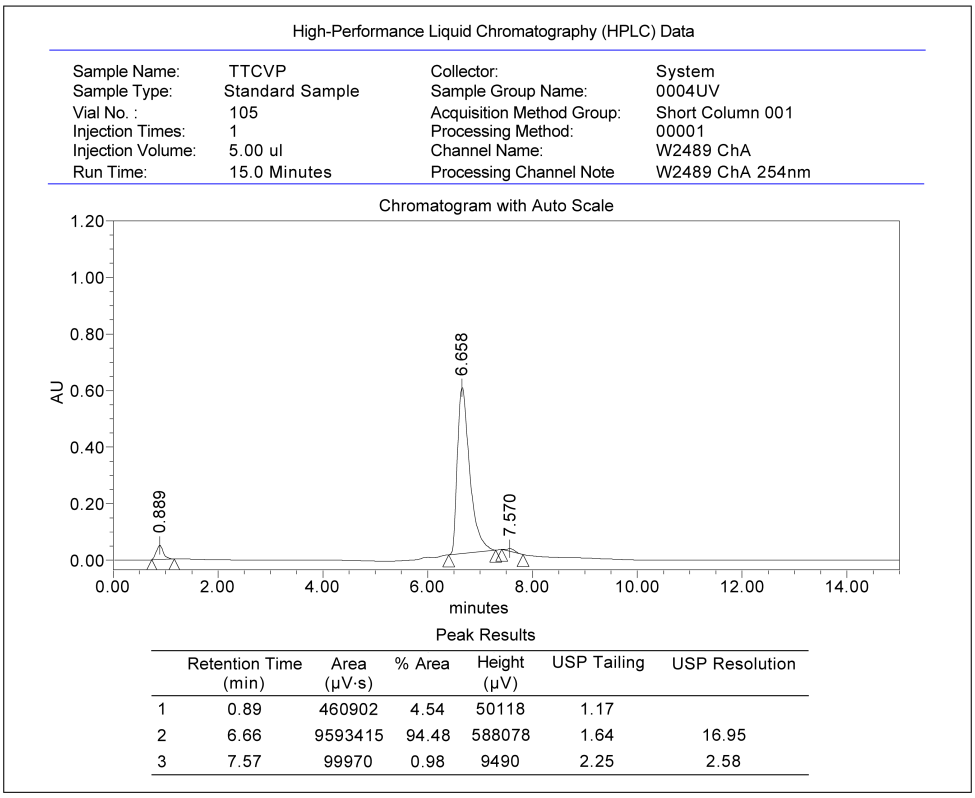

	Retention Time (min)	Area (μV·s)	% Area	Height (μV)	USP Tailing	USP Resolution
1	0.89	460902	4.54	50118	1.17	
2	6.66	9593415	94.48	588078	1.64	16.95
3	7.57	99970	0.98	9490	2.25	2.58

Figure S18. Synthesis and Characterization of TTCVP. Synthesis route of TTCVP (A) and HPLC chromatogram of TTCVP with UV detection at 254 nm (B).

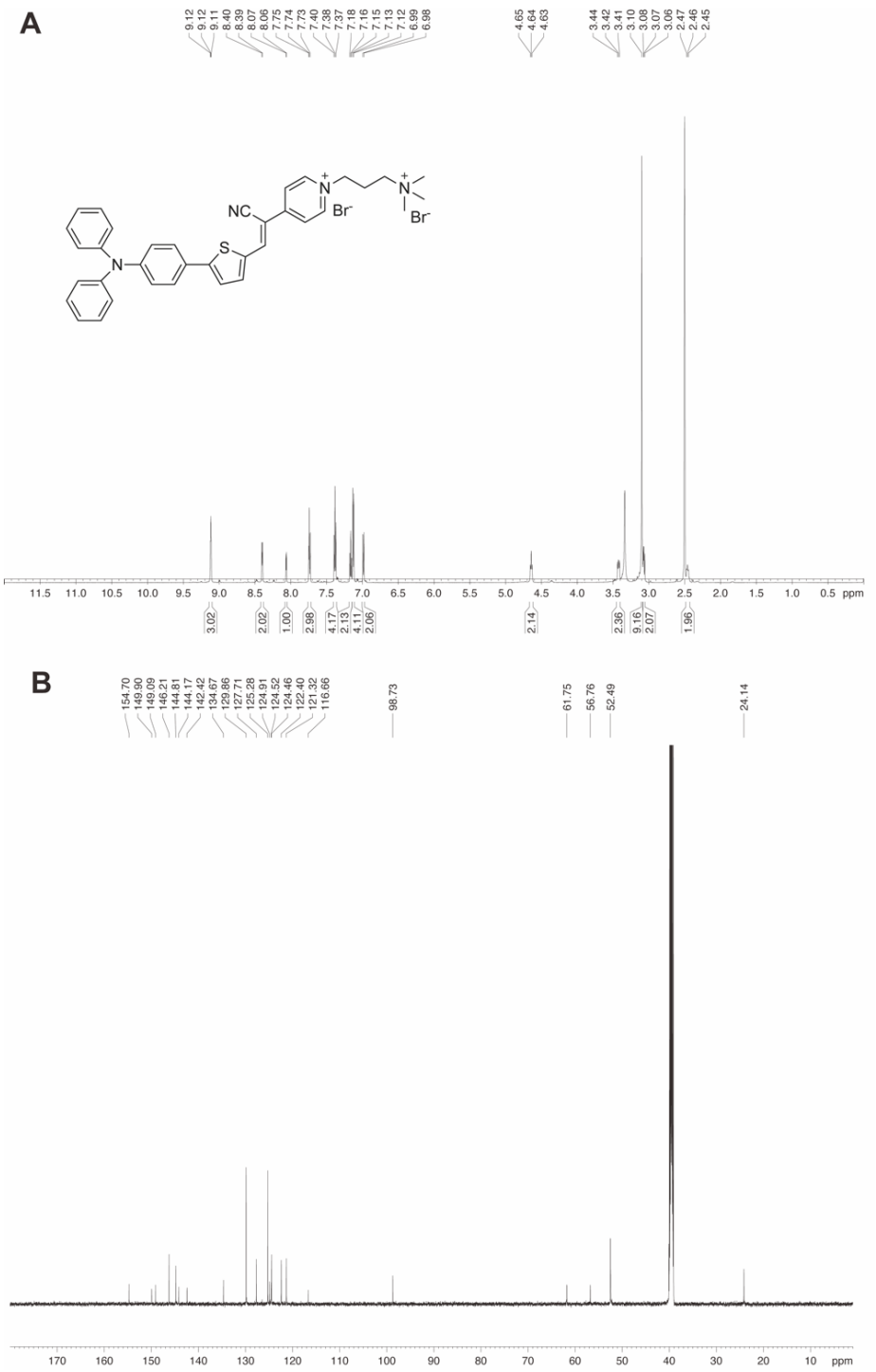

Figure S19. NMR Spectra of TTCVP. ^{1}H NMR (600 MHz, DMSO-$_{d6}$) spectrum of TTCVP (A) and ^{13}C NMR (150 MHz, DMSO-$_{d6}$) spectrum of TTCVP (B).

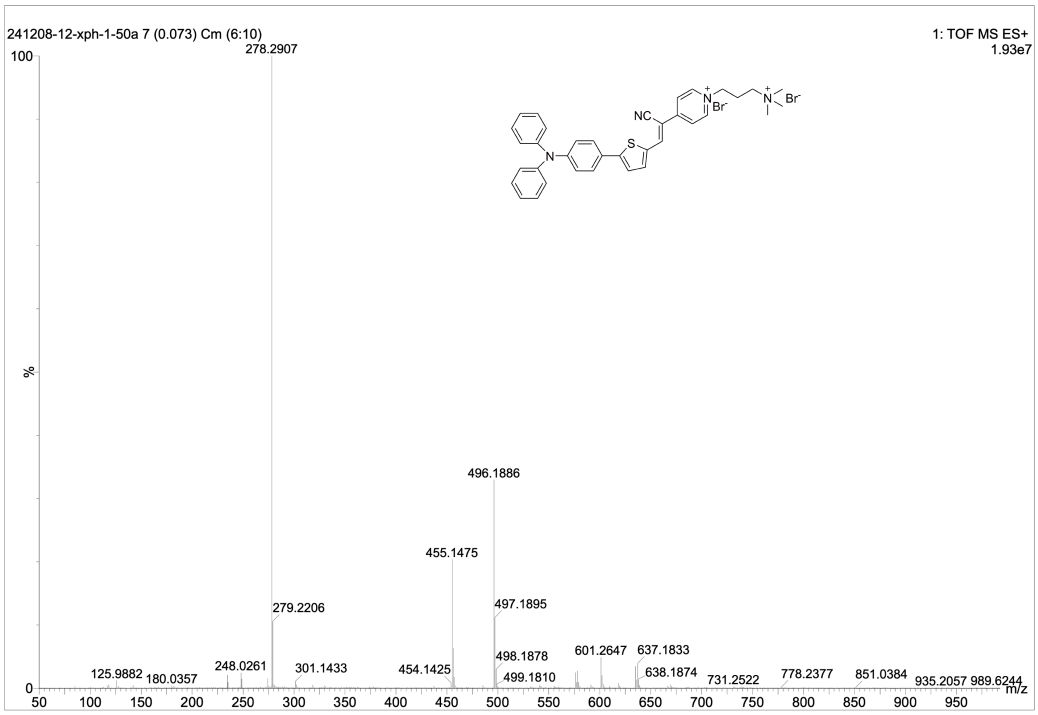

Figure S20. HRMS Spectrum of TTCVP.